JOURNAL OF PETROLEUM GEOMECHANICS
(JPG)

Evaluation of the production rate efficiency of the deformable oil reservoir using the enhanced Multiscale method

Ehsan Taheri[1*]; Ahmadreza Kodaiari[2]; Kamran Gostasbi[3]

1. Assistant Professor; Department of Stone Mechanics, Tarbiat Modares University, Tehran, Iran
2. Ph.d. student; faculty of engineering, Tarbiat Modares University, Tehran, Iran

3. Associate Professor Tarbiat Modares University, Engineering and Technical Department

Received: 04 Agust 2021; Accepted: 08 April 2022

Doi: 10.22107/jpg.2022.298259.1149

Keywords

Multiscale
Production rate
Geomechanics
Deformation
Oil reservoir

Abstract

Petroleum reservoirs contain many physics that play an important role in multiple scales. Fluid flow and deformation of the solid-phase are the main physics that influence the production rate. In the present paper, the fluid transport and deformation of porous media are determined through separate frameworks on different scales. The enhanced Multiscale Multiphysics Mixed Geo-Mechanical Model (EM3GM) has been developed and utilized to determine the production rate of deformable reservoirs. The EM3GM not only contains conservative aspects of Multiscale Finite Volume (MSFV) in fluid flow but also develops with properties of Elastic-Plastic framework in the solid domain. Finally, in order to show the accuracy of the model and also to reveal the effect of the plastic deformations in production rate, indicative test cases were analyzed, and reasonable results were achieved. The plastic deformation will lead to a decrease in oil production rate with respect to energy losses during plastic deformation, which is closer to the real situation. The numerical results show that neglecting solid deformation could overestimate the production rate from one to four times higher at the earlier stage of production for the hard rock, and this amount would be increased for the loose rock with respect to higher energy loss.

1. Introduction

Many physical phenomena, such as flow in oil and gas petroleum reservoirs and mechanical behavior of composite material, occur on a wide variety of physical scales (Aarnes, Kippe, Lie, & Rustad, 2007). The fine-scale analysis of such kinds of media with several scales of heterogeneities is extremely difficult for the traditional methods. Therefore, with the trend of capturing the fine-scale effect on the coarse scales, Multiscale models were developed in different fields of physics and materials. Methods are based on homogenization theory (Kanoute, Boso, Chaboche, & Schrefler, 2009). In oil and gas reservoir fields, however, recent developments of geological models provide detailed specifications for porous media that are essential for accurate reservoir fluid simulations (Zhang & Liu, 2014). Implementation of the fine texture of these

• *Tehran; Tarbiat Modares University; Department of Stone Mechanics, T: 09122437665, Email: e_taheri@modares.ac.ir*

geological aspects by conventional simulators is too expensive or impossible (Durlofsky, 2003). To fill aforementioned gap, various models were developed to upscale these geological models. Nevertheless, in upscaling methods, the loss of information caused by coarsening together with the lack of realistic assumptions about the fine-scale distribution of the system variables will result in inaccurate results (Hou & Wu, 1997). In this paper, among various types of Multiscale methods, with respect to physical essence and locally conservativeness and plastic deformations, the enhanced Multiscale finite volume (MSFV) base is developed (Taheri, 2015) & (Sadrnejad, Ghasemzadeh, & Taheri, 2014). This method originated from the pioneering idea of Babuška and Osborn (1983) in a finite element framework (Babuška & Osborn, 1983). The method was extended by Hou and Wu in 1997 for general heterogeneities in composite materials and porous media. Jenny and colleagues in 2003 applied this idea in the finite volume framework with a locally conservative nature for subsurface flow simulation (Jenny, Lee, & Tchelepi, 2003). The MSFV method provides locally conservative velocity fields, which is crucial for accurately solving the saturation transport equations (Jenny, Lee, & Tchelepi, 2003). In the recent decade, the MSFV framework was increasingly promoted from single phase to multiphase flow with complex physics (Jenny, Lee, & Tchelepi, 2004) and (Jenny & Lunati, 2009). Furthermore, a local assumption of MSFV approaches the actual condition by implementing iterative boundary conditions (Jenny & Lunati, 2009). However, all of these developments are related to the flow equation. On the other hand, the deformation of porous media is a major concern in some reservoirs. Accurate modeling of a reservoir requires both an understanding of the porous flow and knowledge of reservoir stress and displacement. In this regard, many type of research revealed the important role of geomechanics in petroleum reservoir engineering (Sokolova, Bastisya, & Hajibeigi, 2019). Surface subsidence can damage the surface installations and wellbore instability and can also create environmental problems. So, the development of techniques for estimating soil deformation in a computationally efficient manner is a major concern (Sadrnejad, Ghasemzadeh, & Taheri, 2014). Multiscale methods were developed for the simulation of porous oil reservoirs using lower computational costs (Taheri, 2015) & (Sadrnejad, Ghasemzadeh, & Taheri, 2014). Deformations have an impact on the uppermost facilities, flow path, and production efficiency of reservoirs. Therefore, the Multiscale Multiphysics Mixed Geo-Mechanical Model (M3GM) was developed by Taheri (Sadrnejad, Ghasemzadeh, & Taheri, 2014). In this model, solid deformations were calculated using elastic equations. Next, the effect of the surrounding rocks on the oil reservoir deformation in M3GM was developed by Sadrnejad et al, in 2014 (Taheri, 2015), which is the base of this paper. Using an accurate elastoplastic model for calculating the deformations of the solid-phase of oil reservoirs could be a powerful tool to achieve more accurate results. Additionally, Taheri et al, in 2015 discussed the combination of Multiscale finite-volume (MSFV) and finite-element frameworks for simulation of fluid transport and soil deformation, and they used a new method which was the treated dual-volume boundary condition (TDVBC) (Taheri, Sadrnejad, & Ghasemzadeh, 2015). Moreover, utilizing constitutive models for coupling hydraulic and mechanical behaviors of unsaturated soils and rocks is an interesting subject in geotechnical studies. In this regard, the plastic framework was developed by Moghadam and colleagues for considering Elastic and plastic deformation in an implicit approach (Moghadam, Taheri, & Ghoreishian, 2022). Combining these two frameworks resulted from the Enhanced Multiscale Multiphasic Mixed Geomechanical Model (EM3GM). In addition, an elastoplastic model is added by Ghasemzadeh and colleagues for increasing the accuracy of (M3GM) (Ghasemzadeh & Sanaye Pasand, 2019). The Improved Multiscale Multiphysics Mixed Geomechanical Model (IM3GM) was introduced by simulating the effects of the surrounding area of reservoirs, and reasonable agreements were obtained (Ghasemzadeh, 2019). Finally, to estimate the errors in the MSFV solutions for continuous problems, a heterogeneous two-dimensional problem with a continuous permeability field was designed and solved analytically by Mazlumi et al, (Mazlumi, Mosharaf-Dehkordi, & Dejam, 2021). In the present research, deformation of porous media is implemented in an iterative Multiscale framework, and the role of mechanical behavior of the rock reservoir rock in the production rate is investigated. In the presented framework, all advantages of the Multiscale framework are preserved. In order to have a better prediction of soil behavior and its effect on an oil production rate, a finite element method with quadratic elements is applied. In this paper, first, the governing equation and mass and momentum balance of fluid and solid-phases are presented. In the second part, a Multiscale framework for fluid flow and finite element formulation of the solid-phase is illustrated. An iterative strategy with the Newton-Raphson method is explained to clear the interaction of solid and fluid phases. Finally, indicative test cases are analyzed, and the role of plastic strain on the production rate is determined.

2. Methodology and Approaches

In this work, two compressible fluids flow with deformable solid skeleton are considered. Without loss of generality, the simplified form of mass conservation law demonstrated by Lewis & Schrefler in 1998 is taken into account.

$$\frac{D^s}{Dt}(\phi S_\alpha \rho_\alpha) + \nabla(\phi S_\alpha \rho_\alpha \boldsymbol{w}_\alpha) + \phi S_\alpha \rho_\alpha \nabla \boldsymbol{v}_s = \dot{m}_\alpha \tag{1}$$

Where ϕ is the porosity, ρ_α the phase density, S_α the phase saturation, $\boldsymbol{v}_\alpha$ the velocity of phaseα, relative velocity $\boldsymbol{w} = \boldsymbol{v}_\alpha - \boldsymbol{v}_s$and $\dot{m}_\alpha$denotes sink and source terms.

By taking sum over all phases, and implementing the Linear momentum balance equation of fluid phases into fluid mass balance, one may obtain (Taheri, 2015):

$$\phi \frac{D^s}{Dt}\sum_{\alpha=1}^{n_p} S_\alpha \rho_\alpha + \sum_{\alpha=1}^{n_p} S_\alpha \rho_\alpha \frac{D^s \phi}{Dt} + \sum_{\alpha=1}^{n_p} \nabla.(\rho_\alpha \boldsymbol{\lambda}_\alpha.[-\nabla p + \rho_\alpha g]) + \sum_{\alpha=1}^{n_p} \phi S_\alpha \rho_\alpha \nabla \boldsymbol{v}_s = \dot{m}_\alpha \tag{2}$$

where $\boldsymbol{\lambda}_\alpha$ is phase mobility tensor $\boldsymbol{\lambda}_\alpha = \frac{\boldsymbol{K}\mathrm{kr}_\alpha}{\mu_\alpha}$, K is the absolute permeability tensor, kr_α is relative permeability and μ_α is the phase viscosity.

On the other side, the equilibrium of the solid-phase can be described in the following form:

$$\nabla.\boldsymbol{\sigma} + \rho\boldsymbol{g} = 0 \quad (3)$$

In above formula $\boldsymbol{\sigma}$ is a total stress vector. However, in soil mechanics effective stress is considered instead of total stress. The relation between total and effective stress is instated by Eq.(4).

$$\boldsymbol{\sigma}' = \boldsymbol{\sigma} - \boldsymbol{I}p \quad (4)$$

Where $\boldsymbol{\sigma}'$ is the effective stress, $\boldsymbol{I}$ is the Kronecker delta tensor, and p is the fluid pressure By considering relation between strain and deformation, definition of volumetric strain and solid-phase velocity will lead (Taheri, 2015):

$$\varphi\frac{D^s}{Dt}\sum_{\alpha=1}^{n_p} S_\alpha\,\rho_\alpha + \sum_{\alpha=1}^{n_p} S_\alpha\,\rho_\alpha\frac{D^s\varphi}{Dt} + \sum_{\alpha=1}^{n_p}\nabla.\left(\rho_\alpha\frac{\boldsymbol{K}\mathrm{kr}_\alpha}{\mu_\alpha}.\left[-\nabla p + \rho_\alpha g\right]\right) + \sum_{\alpha=1}^{n_p}\varphi S_\alpha\rho_\alpha\frac{\varepsilon_{vol}}{\Delta t} = \dot{m}_\alpha \quad (5)$$

Since two fluid phases are taken into consideration, two mass balances exist. However, phase saturations are subjected to the following constraint.

$$\sum_{\alpha=1}^{n_p} S_\alpha = 1 \quad (6)$$

By utilizing Eq. (6), Calculating only one mass balance will be adequate.

3. Multiscale Multiphysics Mixed Geo-Mechanical Model.

Many physical phenomena occur in multiple length scales. So, in this research, the discretization is derived based on the Multiscale nature of the fluid flow in reservoirs. The basic principles and theory of derivation are comprehensively illustrated by Taheri in 2015 and Sadrnejad and colleagues in 2014, and interested readers could refer to them (Taheri, 2015; Sadrnejad, Ghasemzadeh, & Taheri, 2014). However, in a summarized manner by implicit Euler time discretization of Eq. (5) one may obtain:

$$\frac{\boldsymbol{\varphi}^{n+1}}{\boldsymbol{\Delta t}} + \frac{-\boldsymbol{\varphi}^{n}}{\boldsymbol{\Delta t}}\sum_{\alpha=1}^{n_p}\boldsymbol{B}_\alpha^{n+1}\boldsymbol{\rho}_\alpha^{n}\boldsymbol{S}_\alpha^{n} - \sum_{\alpha=1}^{n_p}\boldsymbol{B}_\alpha^{n+1}\boldsymbol{\nabla}.\left(\boldsymbol{\rho}_\alpha^{n+1}\boldsymbol{\lambda}_\alpha\left(\boldsymbol{\nabla p}^{n+1} - \boldsymbol{\rho}_\alpha^{n+1}\boldsymbol{g\nabla z}\right)\right) + \boldsymbol{\varphi}^{n+1}\frac{\boldsymbol{\varepsilon}_v^{n+1} - \boldsymbol{\varepsilon}_v^{n}}{\boldsymbol{\Delta t}} = \boldsymbol{q}_t \quad (7)$$

Where $q_t = \sum_{\alpha=1}^{n_p} q_\alpha$ is total volumetric sink/source term and B_α is formation volume factor (the inverse of phase density).

Linearization of this equation results in the iterative linear pressure equation.

$$-\phi^{v}\sum_{\alpha=1}^{n_p}\frac{\partial B_\alpha}{\partial p}\Big|^{v}\cdot\rho_\alpha^n S_\alpha^n(p^{v+1}-p^{v})-\sum_{\alpha=1}^{n_p}B_\alpha^{v}\nabla.(\rho_\alpha^{v}\boldsymbol{\lambda}_\alpha\nabla p^{v+1}) = \frac{-\phi^{v}}{\Delta t}+\frac{\phi^{n}}{\Delta t}\sum_{\alpha=1}^{n_p}B_\alpha^{n+1}\rho_\alpha^n S_\alpha^n+q_t-\sum_{\alpha=1}^{n_p}B_\alpha^{v}\nabla.(\rho_\alpha^{v\,2}\boldsymbol{\lambda}_\alpha g\nabla z) - \phi^{v}\frac{\varepsilon_v^{v}-\varepsilon_v^{n}}{\Delta t} \quad (8)$$

The above linearized equation will converge to Eq. (7) while pressure iteration proceeds. New and old iteration levels are shown by superscript $v+1$and v respectively.

In contrast to the work of Hajibeigy and Jenny in 2009, deformation of the solid skeleton is treated with respect to effective stress concept, which is essential in geomechanics (Taheri, 2015).

MSFV framework relies on two imposed grids, namely coarse grid (solid line in Fig. 1) and dual coarse grid (dashed line in Fig. 1). Coarse grid includes M coarse cells$\boldsymbol{\Omega}_k \in [1, M]$ and dual coarse grid, contains N dual volume$\boldsymbol{\Omega}^h \in [1, N]$. As shown in Fig. 1, the size of these two grids could be much larger than the underlying fine cells extracted from the geological model.

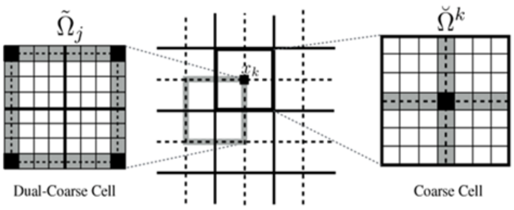

Fig. 1: Illustration of coarse grid (solid line), dual coarse grid (dashed line) and underlying fine grid, also shown is dual volume boundary.

MSFV framework consists of two main operators. First, operator upscale the fine grid geological property with respect to integration over fine pressure obtained from two sets of shape function i.e., basis functions $\boldsymbol{\Phi}_k^h$ and correction function$\boldsymbol{\Phi}^h$. Second operators also utilize these two sets in order to obtain fine scale pressure and corresponding fine scale flow over each coarse volume to obtain conservative fine pressure with original resolution. However, different from the classical finite element these functions are not analytical functions but from the mathematical point of view, general and particular solutions of Eq. (8) with localized assumption.

In a more precise illustration, basis and correction functions are numerical solutions of homogenous and in-homogenous parts of Eq. (9) with respect to reduced problem boundary conditions on the borders of each dual, volume as shown in Fig. 1.

$$(\tilde{\boldsymbol{n}}^h.\nabla)\big((\lambda_t.\nabla\boldsymbol{\Phi}_k^h).\tilde{\boldsymbol{n}}^h\big)=0 \quad (9)$$

$$(\tilde{\boldsymbol{n}}^h.\nabla)\big((\lambda_t.\nabla\boldsymbol{\Phi}^h).\tilde{\boldsymbol{n}}^h\big) = RHS^{v} \quad (10)$$

Where $\tilde{\boldsymbol{n}}^h$ being the unit normal vector pointing out of $\partial\boldsymbol{\Omega}^h$. Boundary conditions are given at the dual grid nodes x_l by $\boldsymbol{\Phi}_k^h(x_l) = \delta_{kl}$, $\boldsymbol{\Phi}^h\ (x_l) = 0$

It's worth mentioning that other physical phenomena such as capillary mass exchange between phases, etc. could be treated routinely in RHS of Eq. (10) with the contribution of correct functions. By superposition of these two sets of shape functions, fine scale pressure could be achieved through the approximation:

$$p_f(x) \approx p'(x) = \sum_{h=1}^{N}\left[\sum_{k=1}^{M} \boldsymbol{\Phi}_k^h(x)\bar{p}_k + \boldsymbol{\Phi}^h\ (x)\right] \tag{11}$$

Where $\bar{p}_k$ are the pressure values at the center nodes of each coarse volume x_k, as depicted in Fig. (1) Substituting Eq. (11) in Linearized pressure equation and integrating over coarse volumes and applying the gauss theorem leads will result results in an iterative nonlinear system (Taheri, 2015):

$$\boldsymbol{A}_{lk}\boldsymbol{p}_k^{v+1} = \boldsymbol{b}_l^v \tag{12}$$

For $\boldsymbol{p}_k^{v+1}$ with

$$\boldsymbol{A}_{lk} = \sum_{h=1}^{N}\left(\int_{\bar{\boldsymbol{\Omega}}} \frac{C_c}{\Delta t}\boldsymbol{\Phi}_k^h d\Omega - \int_{\partial\bar{\boldsymbol{\Omega}}_l} (\lambda_t.\nabla\boldsymbol{\Phi}_k^h).\tilde{\boldsymbol{n}}_l d\Gamma\right) \tag{13}$$

And

$$b_l^v = \int_{\bar{\boldsymbol{\Omega}}}\left(RHS^v + \frac{C_c}{\Delta t}p'^v\right)d\Omega - \sum_{h=1}^{N}\left(\int_{\bar{\boldsymbol{\Omega}}} \frac{C_c}{\Delta t}\boldsymbol{\Phi}^{h^v} d\Omega - \int_{\partial\bar{\boldsymbol{\Omega}}} \lambda_t.\nabla\boldsymbol{\Phi}^{h^v}.\tilde{\boldsymbol{n}}_l d\Gamma\right) \tag{14}$$

Implementing $\boldsymbol{p}_k^{v+1}$ in Eq. (11) results in the fine scale pressure value p'^{v+1}. The iterative procedure is continued until convergence obtains. i.e., $\|p'^{v+1} - p'^v\| < \beta$, where β is the convergence limit. However, this pressure field is not conservative, which is crucial for solving transport equations, so further steps are needed. As already mentioned, this pressure filed is applied in order to obtain fine scale flow over each coarse volume. In a detailed statement, Eq. (8) is solved with the Neumann boundary condition obtained from a fine scale pressure field, i.e., p'' which is used for solving saturation equation.

4.Solid-phase discretization and Elastoplastic framework

In order to discretize soil momentum balances i.e., Eq. (4) standard Galerkin method is applied. Neglecting body force and considering boundary conditions, and utilizing finite element formulation, which results in the nonlinear system:

For $\hat{\boldsymbol{u}}$ with

$$\boldsymbol{K} = \left[\int_{\Omega} \boldsymbol{B}^T \boldsymbol{D}_{ep} \boldsymbol{B} \quad d\Omega\right] \tag{15}$$

And

$$\boldsymbol{F} = -\int_{\Gamma^N} \boldsymbol{N}_u^T \bar{t} d\Gamma + \int_{\Omega} \boldsymbol{B}^T (p\boldsymbol{m}) d\Omega \tag{16}$$

Where $\hat{\boldsymbol{u}}$is deformation vector, $\boldsymbol{B}$is the consistent tangent of the skeleton multiplied by shape functions, $\boldsymbol{D}_{ep}$ is Elastoplastic modules matrix, Matrix $\boldsymbol{K}$ and the first term on the RHS is calculated by conventional finite element method. Second term on the RHS, namely F2 is obtained by integrating over all fine cells encapsulated in each course volume.

$$\boldsymbol{F}_2 = \sum_{i=1}^{i=nfs} B_i^T \, p_i.m.A \tag{17}$$

In the above formula p_i is fine scale pressure and A is the area of each fine cell. The EM3GM is nonlinear since the value of integral is calculated via pressure obtained based on previous deformation status. The basic principles and detailed procedure of discretization are thoroughly explained in the ref. (Taheri, 2015).

In this research, Newton-Raphson method is applied in each sequential loop which will be explained in the next section. Moreover, the deformations in soils and rocks are both elastic and plastic. In the previous framework developed by Taheri, 2015 and Sadrnejad, 2014, the elastic strains were taken to account. In this research, however, not only will the elastic strain be considered in the present framework, but also the plastic strain will also be regarded in a systematic approach. In this regard, the plasticity theory was enhanced with a sub-loading surface developed by Moghadam and colleagues (Moghadam, Taheri, & Ghoreishian, 2022). will be employed. However, based on the plasticity theory, strains are decomposed in the elastic and the plastic portions.

$$d\varepsilon = d\varepsilon_e + d\varepsilon_p \tag{18}$$

In the following, volumetric modulus K and shear modulus $G$are defined to introduce the elastic behavior of the model:

$$K = \frac{vp'}{k} \tag{19}$$

$$G = \frac{3(1-2\mu)}{2(1+\mu)} K \tag{20}$$

In mentioned equations, $v = (1+e)$ is the specific volume, k is the loading – unloading line slope in the $v - ln\, p'$plane, and $\mu$is the Poisson’s ratio. In the present model, to predict and simulate the behavior of the rock accurately, the concept of bonding surface plasticity has been utilized for a smooth transition from elastic to plastic state of the rock. Based on bonding surface plasticity, the plastic deformations are taken place readily after loading. According to this theory, the present model employs an inner surface (as the loading surface) and an outer surface (as the bonding surface), with the current stress point always passing through the loading surface. A radial mapping rule is used to place the image of the current stress point on the bonding surface. Fig. 2 shows the loading and bonding surfaces on the $q-p'$ space.

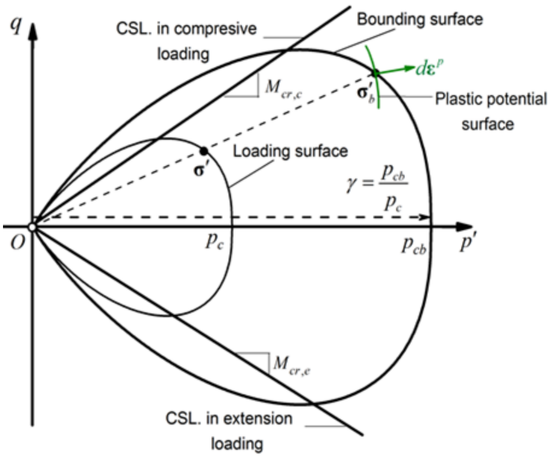

Fig. 2: Loading and bonding surface and radial mapping rule

It is assumed here that the loading surface and the bonding surface have a similar shape and are defined by the unified yield function:

$$F(\boldsymbol{\sigma}, p_c) = \left(\frac{q}{Mp'}\right)^N + \frac{ln(\frac{p'}{p_c})}{ln(R)} \qquad (21)$$

Due to the similarity of the loading surface and the bonding surface, the image stress point on the bonding surface can be calculated using the similarity ratio:

$$\gamma = \frac{\boldsymbol{\sigma}}{\boldsymbol{\sigma}_b} = \frac{p_c}{p_{cb}} = \frac{p'}{p'_b} = \frac{q}{q_b} \qquad (22)$$

In the above equation γ defines the ratio between the size of loading and bonding surfaces, and it is known as a similarity ratio. The similarity ratio will be determined based on the distance between the loading surface and the bonding surface to create plastic strains. To this end, an evolution rule was considered for the similarity ratio according to following equation:

$$d\gamma = -U\, ln(\gamma)\|d\boldsymbol{\varepsilon}^p\| = -U\, ln(\gamma) d\lambda \qquad (23)$$

Where $U$is a material constant and $d\lambda$ is the plastic multiplier.
The implementation of the constitutive models needs numerical integration schemes. From a computational point of view, the implicit integration scheme based on the return mapping algorithm has been employed owing to its convergence and stability when compared to other schemes.
There are two steps to this algorithm: elastic predictor and plastic corrector. The following is a more detailed description of this algorithm:

i. Elastic predictor phase:

In the elastic predictor phase, the stress is calculated based on elastic behavior at the beginning of each time step corresponding to the relevant strain.

$$\boldsymbol{\sigma}^{trial} = \boldsymbol{\sigma}_n + \boldsymbol{D}_{n+1}.\, d\boldsymbol{\varepsilon}_{n+1} \quad (24)$$

In the above equation, $n+1$ corresponds to the current time step and n is related to the previous time step. $\boldsymbol{\sigma}^{trial}$ is the stress predictor of the elastic state, and it is the trial stress. In the next step, this stress should be modified in the plastic corrector phase based on elastic-plastic equations. $\boldsymbol{D}_{n+1}$ is the elastic modulus matrix in the current step.

ii. Plastic corrector phase:

In this phase, the trial stress that was calculated in the previous step should be modified with respect to the flow rule, hardening rule, and also the evolution rule in a way that consistency conditions will be satisfied.

Equilibrium equation:

$$\boldsymbol{\sigma}_{n+1} = \boldsymbol{\sigma}_n + \boldsymbol{D}_{n+1}(d\boldsymbol{\varepsilon}_{n+1} - d\boldsymbol{\varepsilon}^p_{n+1}) \quad (25)$$

Hardening rule:

$$p_{cb,n+1} = p_{cb,n}\, exp\left(\frac{v_n}{\lambda-\kappa}\left(d\varepsilon^p_v\right)_{n+1}\right) \quad (26)$$

Evolution rule:

$$\gamma_{n+1} = \gamma_n - U\, ln(\gamma_{n+1})d\lambda \quad (27)$$

Loading surface function:

$$F(\boldsymbol{\sigma}'_{n+1}) = \left(\frac{q_{n+1}}{M_{cr}p'_{n+1}}\right)^N + \frac{ln\left(\frac{p'_{n+1}}{\gamma_{n+1}p'_{cb,n+1}}\right)}{ln(R)} = 0 \quad (28)$$

Finally, fulfillment of Eq. (36-39) simultaneously will result the nonlinear system of equations with ahead unknowns$[\boldsymbol{\sigma}_{n+1}, p_{cb,n+1}, \gamma_{n+1}d\lambda]$. The mentioned system of equations will be solved by employing the Newton-Raphson method. The procedure of solving the system of equations is illustrated in the table. The stress calculation procedure using the Euler implicit scheme is depicted in Fig. 3.

The basic principles and theoretical background are comprehensively explained by the author in ref. (Moghadam, Taheri, & Ghoreishian, 2022) and the interested reader could refer to them to understand the basic parameters and their roles.

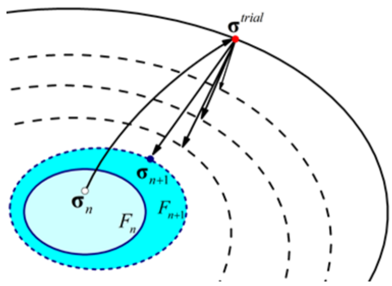

Fig. 3: Return mapping projection

5. Framework interaction

The iterative two-way solution method is used to create the interaction between the framework of the Multiscale and the finite element method. In this regard, the fluid and solid equation system are connected by the Newton-Raphson iteration loop. The converged Multiscale pressure is used to input the finite element method, which is used in the space of finite element cells. For convergence, the calculated pressure equations return to the calculation cycle. At the beginning and

after each time step, in the first stage, the phase mobility capability is controlled. After controlling this value and if the phase mobility threshold value exceeds its allowable limit, Basic functions are recalculated and updated. If a phase mobility change is within the allowable range, the problem enters the coupling loop of the other two phases, liquid and solid. After this operation and extraction of the main functions, the system of equations is formed, and a coefficient matrix is obtained. Next, large-scale pressures are extracted, and then the fine scale pressure is obtained, this is where the Elastoplastic framework comes into account. The output of the mass balance equation is pressure. The output of the equilibrium equation is the phase deformation of the solid-phase. In the basic M3GM model, this deformation was returned to the mass equation to converge. However, in the present paper, plastic strain is also calculated based on the theory of plasticity, as mentioned in section 4. In this regard, the state of the stress is controlled within the sub-loading surface. In order to have an overview of the procedure, the algorithm of fluid flow interaction with the deformable porous media is shown in Fig. 4
.

EM^{3}GM Pseudo Code	***Eqs.***
Start of simulation	
n = 1	
do	
Loop I: Timestep	
$\boldsymbol{v_c = 1, p^{v_c} = p^n}$	
do	
Loop II: Nonlinear Newton iterative coupling	
$\boldsymbol{v_p = 1 : p^{v_p} = p^{v_c}}$	
do	
Loop III: Pressure iteration	*(11-14)*
Update correction functions	
Solve linearized pressure equation	
$\Rightarrow \boldsymbol{p^{v_{p+1}}}$	
$\boldsymbol{v_p = v_p + 1}$	
Until (convergence of nonlinear pressure equation)	
Geo mechanical plastic system	*(25-28)*
Solve deformation equation	
Plastic corrector phase	
Calculate volumetric strain and updating porosity	
$\boldsymbol{p^{v_{c+1}} = p^{v_p}}$	
Until (convergence of system of pressure and geo-mechanical system)	
Construct conservative fine fluxes	
Solve transport equation	
$\boldsymbol{S_\alpha^{n+1} = S_\alpha^n}$	
Until (end of simulation)	

Fig. 4: The algorithm of fluid flow interaction with the deformable porous media

6. Numerical results

6.1. Five-spot multiphase flow with deformation in homogeneous porous media

As a first test case, water injection in oil reservoirs is studied. In this case, a square domain (44 x 44 m) with absolute permeability K=2.5×10^(-13) m^2, and it's initially saturated with oil (S_o=1). As shown in Fig. 5, the water is injected in the lower-left corner, and production occurs in the upper right corner. Each coarse cell contains 11x11 underlying fine cells, so a coarsening factor of121 is considered. The oil-water viscosity ratio is 5. The initial and boundary condition and also geo-mechanical properties of the reservoir rock and fluid are shown in table 1.

To control the accuracy of the model, the pressure field obtained from the present model fine-scale simulation is shown in Fig. 6. It is clear from the figure 6 that the trend and also amount of the pressure filed obtained from the Multiscale model (Left contours) are in good agreement with fine-scale simulations (right contours). It is also form this figure that the pressure field is higher around the injection well, and increases while the injection precedes (from 0.01 Pore Volume Injection (PVI) to 0.1 PVI).

Table 1. The fluid specification and geo-mechanical parameters of the porous media

K	E	v	μ_w	μ_o	ρ_w	ρ_o	ϕ	S_o
$2.5\times10^{-13}m^2$	$5GPa$	0.2	$10^{-3}Pa.s$	$5\times10^{-3}Pa.s$	$1000\frac{kg}{m^3}$	$950\frac{kg}{m^3}$	0.2	1

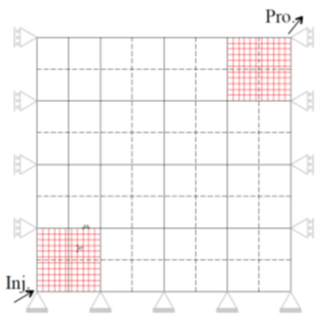

Fig. 5: Setup of the five-spot waterflood problem with a coarsening factor of 121

Moreover, in order to compare the effect of deformation, two simulations were carried out. In the first simulation, deformation is neglected, and only mechanical flow in porous media is taken into account. In the second case, however deformation is taken into consideration. Fig. 7 shows oil production rate for both compressible and incompressible porous media. First, to verify the present model, the result obtained from the previous version of the model (M3GM) is compared with the fine-scale simulation obtained from the Ghoreishian model (Ghoreishian, 2012) (Left side). It is evident from this figure that results are in reasonable agreement. Moreover, it is detectable that considering deformation will lead to a lower production rate. The reason is, that some portion of injection energy is dissipated through deformation. In this regard, the production in incompressible porous media simulation (no energy loss) is overestimated which could lead to an unrealistic production plan. Furthermore, to compare the difference between the elastic and the plastic deformation, the related results from M3GM (considering elastic deformation) and EM3GM (considering elastoplastic deformation) are shown in Fig. 7 (Right side). As shown in this figure, when plastic deformation is regarded as close to the real situation, the oil production rate decreases. The reason is that the energy loss is increased when plastic deformation is contemplated.

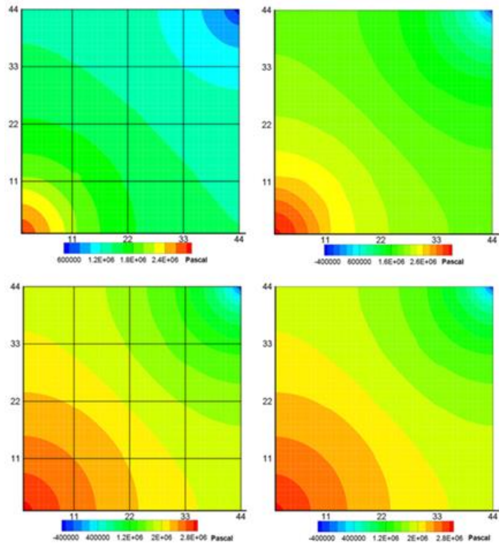

Fig. 6: pressure field obtained from fine-scale simulation using 44x44 fine cells (right) And from EM3GM using 4x4 coarse cells (left) after 0.01PVI (top) and after 0.1PVI (bot.)

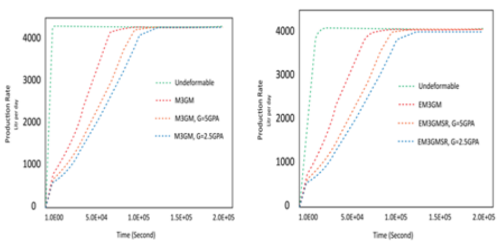

Fig. 7: production rate in undeform able and deformable reservoir M3GM (Left), EM3GM (Right)

6.3. Subsidence in heterogeneous porous media

In the previous section, homogeneous porous media was regarded. However, in order to show the capability of the model the EM3GM results will be evaluated in forthcoming cases. In this regard, the permeability pattern of SEP10 and related young’s modulus and relative permeability that are addressed by Sokolova et al. is considered (Sokolova, Bastisya, & Hajibeigi, 2019). The contour of Young's modulus and relative permeability is shown in Fig. 10. The constant loading of 100 Pa is implemented at the top of the porous media, and the Poisson’s ratio of $\upsilon = 0.2$ is regarded. The initial fluid pressure is 100 Pa that is distributed to the entire domain. As shown in Fig. 10, the roller constraint is applied in three directions while, at the north side, the Newman boundary condition is contemplated. The mechanical and hydro-mechanical boundary conditions are also shown in Fig. 10. The resulting pressure and corresponding deformation in Y direction at $t = 0.06s$ are depicted in Fig 11. The fine scale simulation and EM3GM results are shown on the left and right sides, respectively. It is observed from this figure that not only the pressure field is in good agreement with the fine pressure, but also deformations have the same pattern. It is also obvious that neglecting solid deformation could overestimate the production rate from one to four times higher at the earlier stage of production for the hard rock. It is worth mentioning that in this case, the hard rock was regarded, and the plastic energy loss was at a minimum value. So, it is expected that if looser rock is contemplated, the production rate will be more influenced.

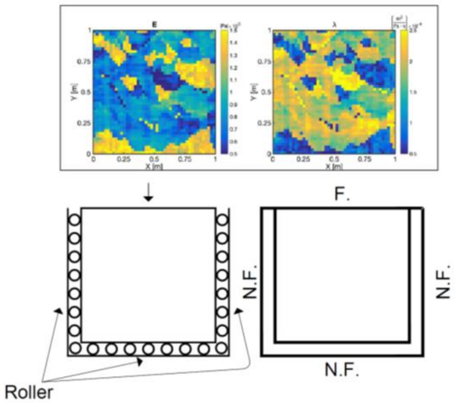

Fig. 10: mechanical and hydro mechanical boundary conditions

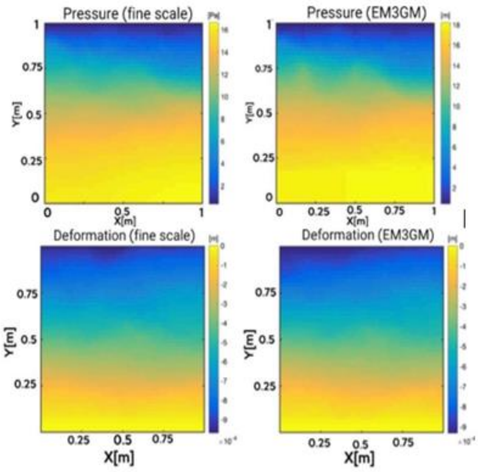

Fig. 11: Simulation results for compaction of heterogeneous media. the comparison of the reference fine-scale (FV) solution for pressure and Y displacement with the corresponding Multiscale solutions obtained with EM3GM method

7. Conclusion

Mature oil management and development of new fields are in need of reservoir simulations. With respect to the Multiscale nature of reservoir rocks and considering any physical phenomenon in its region of influence, the Enhanced Multiscale Multiphysics Mixed Geo-Mechanical Model (EM3GM) for precise simulation of the production rate is presented. By simulation with (EM3GM) not only is the Elastic and Elastoplastic deformation of reservoir rock, but also the surrounding rock is incorporated. It is shown by the model that neglecting the reservoir deformation will overestimate the production rate and could mislead the production strategy. Moreover, the role of considering plastic deformation in production is also revealed. It is also determined that when the plastic deformation is regarded, which is close to the real situation, the production rate will be decreased. This fact could be explained with respect to energy loss during plastic deformation.

NOMENCLATURE

A Fine cell area
$\boldsymbol{u}$ Vector of deformation
B_α Formation volume factor
C_c Compressibility coefficient
C_v Coefficient of consolidation
$\boldsymbol{D}_{ep}$ Module's matrix
E Elastic module
ε_{vol} Volumetric strain
$\boldsymbol{\Phi}_k^h$ Basis function
$\boldsymbol{\Phi}_k^h$ Basis function
$\boldsymbol{\Omega}_k$ Coarse cell
$\boldsymbol{\Omega}^h$ Dual volume
φ Soil porosity
υ Poison ratio
μ_α Phase viscosity
$\boldsymbol{I}$ Identical tensor
K Absolute permeability tensor
β Convergence limit
$\boldsymbol{\varepsilon}$ Strain vector
ρ_α Fluid phase density
$\dot{m}_\alpha$ Sink and source fluid mass
$\boldsymbol{N}_u$ Shape functions
$\tilde{\boldsymbol{n}}^h$ Unit normal vector
p Fluid pressure
p' Dual fine pressure
$p"$ Conservative fine pressure
S_α Fluid phase saturation
t Time
$\boldsymbol{\sigma}'$ Effective stress
$\boldsymbol{\lambda}_\alpha$ Phase mobility tensor

$\boldsymbol{v}_\alpha$ Fluid phase velocity
$\boldsymbol{v}_s$ Solid velocity
$\boldsymbol{w}$ Relative velocity
$\boldsymbol{W}_u^t$ Domain weighted function
$\bar{\boldsymbol{W}}_u^t$ Boundary weighted function

8. References

[1]. Aarnes, J. E., Kippe, V., Lie, K. A., & Rustad, A. B. (2007). Modelling of Multiscale structures in flow simulations for petroleum reservoirs. In Geometric Modelling, Numerical Simulation, and Optimization (pp. 307-360). Springer, Berlin, Heidelberg.
[2]. Kanouté, P., Boso, D. P., Chaboche, J. L., & Schrefler, B. (2009). Multiscale methods for composites: a review. Archives of Computational Methods in Engineering, 16(1), 31-

75.
[3]. Zhang, H., & Liu, H. (2014). A Multiscale computational method for 2d elastoplastic dynamic analysis of heterogeneous materials. International Journal for Multiscale Computational Engineering, 12(2).
[4]. Durlofsky, L. J. (2003, June). Upscaling of geocellular models for reservoir flow simulation: a review of recent progress. In 7th International Forum on Reservoir Simulation Bühl/Baden-Baden, Germany (pp. 23-27). Citeseer.
[5]. Hou, T. Y., & Wu, X. H. (1997). A Multiscale finite element method for elliptic problems in composite materials and porous media. Journal of computational physics, 134(1), 169-189.
[6]. Taheri, E. (2015). Multiscale modeling oil transport in deformable porous media. Phd, K, N toosi university of tech.
[7]. Sadrnejad, S. A., Ghasemzadeh, H., & Taheri, E. (2014). Multiscale multiphysic mixed geomechanical model in deformable porous media. International Journal for Multiscale Computational Engineering, 12(6).
[8]. Babuška, I., and Osborn, E. (1983). Generalized finite elementmethods: Their finite element method for elliptic problems with rapidly oscillating performance and their relation to mixed methods. SIAM J. Numer. Anal. 20, no. 3 510–536.
[9]. Jenny, P., Lee, S. H., & Tchelepi, H. A. (2003). Multi-scale finite-volume method for elliptic problems in subsurface flow simulation. Journal of computational physics, 187(1), 47-67.
[10]. Jenny, P., Lee, S. H., & Tchelepi, H. A. (2004). Adaptive Multiscale finite-volume method for multiphase flow and transport in porous media. Multiscale Modeling & Simulation, 3(1), 50-64.
[11]. Hajibeigi, H. (2011). Iterative Multiscale finite volume method for multiphase flow in porous media with complex physics. ETH, PhD.
[12]. Jenny, P., & Lunati, I. (2009). Modeling complex wells with the multi-scale finite-volume method. Journal of Computational Physics, 228(3), 687-702.
[13]. Sokolova, I., Bastisya, M. G., & Hajibeygi, H. (2019). Multiscale finite volume method for finite-volume-based simulation of poroelasticity. Journal of Computational Physics, 379, 309-324.
[14]. Taheri, E., Sadrnejad, S. A., & Ghasemzadeh, H. (2015). Multiscale geomechanical model for a deformable oil reservoir with surrounding rock effects. International journal for Multiscale computational engineering, 13(6).
[15]. Moghadam, S. I., Taheri, E., Ghoreishian, S. A. (2022). Unified bonding surface model for monotonic and cyclic behaviour of clay and sand, Acta Geotechnica, Accepted.
[16]. Ghasemzadeh, H., & Pasand, M. S. (2019). An elastoplastic Multiscale, multiphysics mixed geomechanical model for oil reservoirs using adaptive mesh refinement methods. International Journal for Multiscale Computational Engineering, 17(4).
[17]. Ghasemzadeh, H. (2019). Multiscale multiphysic mixed geomechanical model for deformable porous media considering the effects of surrounding area. Journal of Petroleum Geomechanics; Vol, 3(1).
[18]. Mazlumi, F., Mosharaf-Dehkordi, M., & Dejam, M. (2021). Simulation of two-

phase incompressible fluid flow in highly heterogeneous porous media by considering localization assumption in Multiscale finite volume method. Applied Mathematics and Computation, 390, 125649.
[19]. Lewis, R. W., Lewis, R. W., & Schrefler, B. A. (1998). The finite element method in the static and dynamic deformation and consolidation of porous media. John Wiley & Sons.
[20]. Hajibeygi, H., & Jenny, P. (2009). Multiscale finite-volume method for parabolic problems arising from compressible multiphase flow in porous media. Journal of Computational Physics, 228(14), 5129-5147.
[21]. Ghoreishian, S. A. (2012). hydro thermo mechanical model for black oil reservoirs, PH. D. Dissertation, KNTU.